On the Alfvénicity of multifluid force-free current sheets

Zijin Zhang,[1, a)] Xiaofei Shi,[1] Sergei Kamaletdinov,[1] Anton Artemyev,[1] Vassilis Angelopoulos,[1] and Marco Velli[1]
Department of Earth, Planetary, and Space Sciences, University of California, Los Angeles, CA, 90095, USA

The solar wind plasma is replete with transient, intense current sheets - also known as solar wind discontinuities - that play a crucial role in solar wind heating and energetic particle scattering. While these discontinuities share similarities with the classical magnetohydrodynamic (MHD) model of rotational discontinuities, they also exhibit complex kinetic behavior beyond single-species fluid models. A particularly puzzling characteristic is their Alfvénicity, hereby defined as the ratio of the plasma velocity jump to the Alfvén velocity jump across the discontinuity. This ratio is expected to approach ± 1 in the MHD framework, yet observations consistently show much lower values. By altering the effective Alfvén speed, plasma thermal anisotropy can partially reconcile theory with observation. However, it alone is not sufficient to fully explain the above discrepancy. This study presents a theoretical model in which the stress balance and velocity difference are described by the kinetics of interpenetrating ion beams crossing the current sheet. Incorporating a nonzero normal and a guide magnetic field, this multifluid model is more advanced and realistic and can be readily compared with observations. We employ this model to explain the Alfvénicity of discontinuities observed in the inner heliosphere.

I. INTRODUCTION

Solar wind discontinuities are highly localized, transient, and intense coherent structures widely observed in the solar wind[1–4]. These discontinuities exhibit characteristics similar to nonlinear Alfvén waves, as evidenced by the strong correlation between variations in plasma and Alfvén speeds[5–8]. Theoretical models predict that discontinuities may originate from Alfvén wave nonlinear evolution[9,10] or plasma turbulence[11]. The magnetic field configurations of most solar wind discontinuities are best described as force-free current sheets, characterized by a constant magnetic field magnitude B, and a strong rotation of magnetic field direction[12]. Similar current sheets have been observed in the night-side magnetospheres of Earth[13,14], Mars[15,16], Venus[17], Mercury[18], and Jupiter[19], as well as at magnetosphere boundaries (magnetopause)[20,21]. Being quasi-1D plasma structures, force-free current sheets (discontinuities) contain two main magnetic field components, $B_x(z)$ reversing across the discontinuity, and $B_y(z)$ reaching a local maximum at B_x reversal, where z denotes the current sheet normal. This specific magnetic field configuration is of particular interest for magnetic reconnection[22,23] and for scattering of energetic charged particles[24–26].

Figure 1 presents three examples of current sheets observed in the solar wind and at Earth's distant magnetotail. All three examples show the same force-free magnetic field configuration with B_x reversal and B_y peak compensating for the drop in magnetic pressure, $B_x^2/8\pi$ (i.e., the stress balance across the sheet is $B_x^2 + B_y^2 = const$). Several models describe force-free current sheets with $B_z = 0$, where the current sheet configuration resembles a tangential discontinuity (see, e.g., Refs. 36–39). However, when $B_z \neq 0$, the tangential discontinuity models are no longer applicable and an additional stress balance (besides $B_x^2 + B_y^2 = const$) should be satisfied: $\Delta v_{A,x} = \Delta U_x$, where Δ denotes the change across the discontinuity[40] for Alfvén and plasma speeds in the x direction. This balance is not fully satisfied in most observed force-free current sheets (see Fig. 1 and Refs. 5–7). Therefore, the current sheet model should be refined and generalized to incorporate properties beyond the overly simplistic single-fluid MHD discontinuity solution.

A natural next step in the generalization of the single-fluid MHD discontinuity solution is the inclusion of plasma anisotropy, where field-aligned and cross-field plasma pressure components differ, i.e. $P_\parallel \neq P_\perp$. Indeed, such anisotropy can significantly influence both the structure[40] and the dynamics[41,42] of discontinuities. In anisotropic plasmas, the Alfvén speed is modified to $v'_A = v_A\sqrt{1-\mu(P_\parallel - P_\perp)/B^2}$ (see, e.g., Ref. 43). As $P_\parallel$ approaches $P_\perp + B^2/\mu$, corresponding to the firehose instability threshold[44,45], the variation $\Delta v_A \propto \sqrt{1-\mu(P_\parallel - P_\perp)/B^2}$ tends to zero. This suggests that the low ΔU_x magnitudes observed in solar wind discontinuities[5–7] could be attributed to sufficiently large field-aligned anisotropy. However, spacecraft observations cannot detect the anisotropy levels required[46,47] to fully account for the observed discrepancy with theoretical predication $\Delta v'_{A,x} = \Delta U_x$. This inconsistency indicates the need for further generalization of the single-fluid MHD model. One such generalization involves considering a multi-component plasma, where counter-streaming ion populations may significantly reduce the required ΔU_x to achieve stress balance[48]. In this study, we develop a multifluid model to describe the 1D structure of force-free current sheets (discontinuities with $B_z \neq 0$), and compare the model predictions with observations in the solar wind.

a)Electronic mail: zijin@ucla.edu

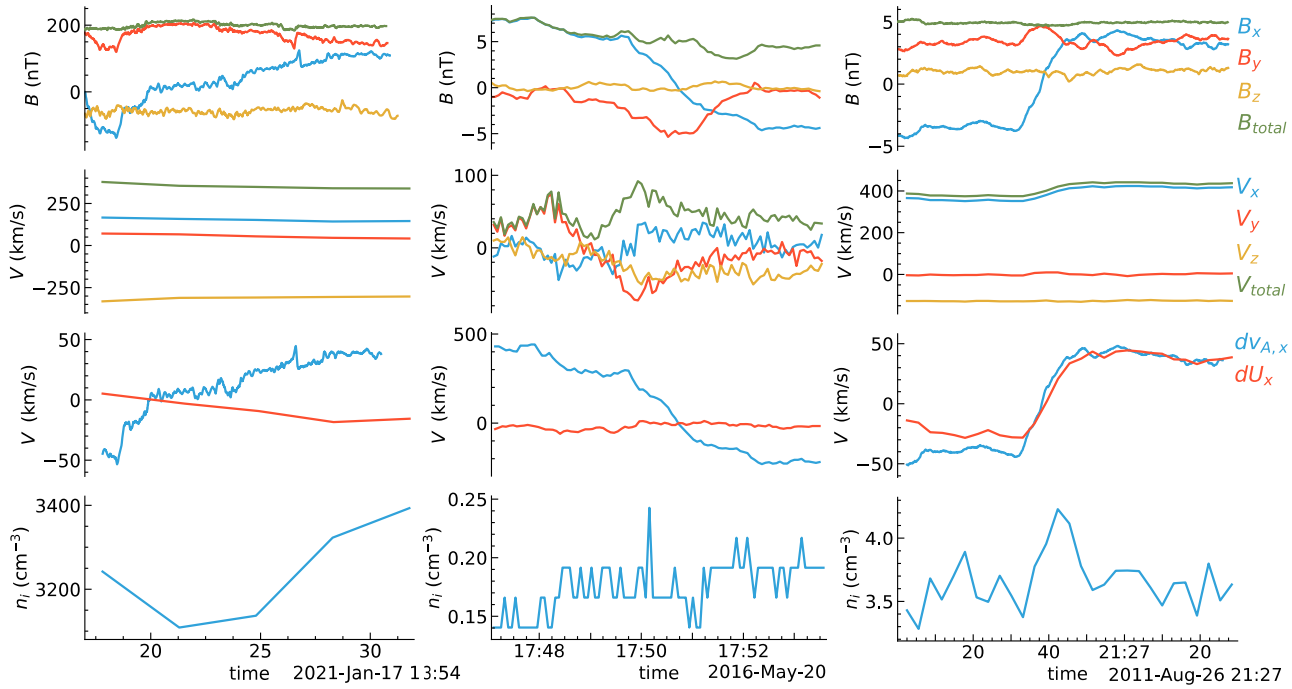

FIG. 1: Three examples of current sheets (discontinuities) observed by the Parker Solar Probe (PSP)[27], ARTEMIS[28], and Wind[29] spacecraft in the LMN coordinate system, each with sub-Alfvénic velocity jumps. From top to bottom, the panels display the magnetic field components,the plasma velocity, the Alfvén velocity in the x-direction (maximum variance direction) with the mean value subtracted (shifted Alfvén velocity), the similarly shifted plasma velocity, and the plasma density. The magnetic field measurements for PSP were obtained using the FIELDS instrument suite[30], while plasma velocity and density data were provided by the SWEAP suite[31]. Similarly, ARTEMIS utilized Fluxgate Magnetometer[32] for magnetic field data and Electrostatic Analyzers[33] for plasma data. For the Wind spacecraft, magnetic field data were collected using the Magnetic Field Investigation instrument[34], and plasma velocity and density were measured by the Solar Wind Experiment[35].

II. MULTIFLUID MODEL

We used a multifluid model for the assumed 1-D quasineutral force-free current sheet equilibrium (satisfying force balance with zero Lorentz force and pressure gradient force). This approach, inspired by Ref. 23 and 49, has the advantage of being analytically tractable while providing the necessary refinements to include kinetic effects of multiple ion species. The fully kinetic approach, which examines the evolution of the velocity distribution function in phase space, is in principle more accurate, but hard to solve analytically for force-free current sheets with $B_n \neq 0$ (see the discussion in Refs. 48 and 50). The multifluid model is a good compromise between the simplicity of the MHD model and the complexity of the fully kinetic model. However, one disadvantage of the multifluid model is that there are more unknowns than equations. This means that the model is underdetermined and requires additional assumptions to be solved. This closure problem is usually addressed by choosing equations of state. Because the force-free current sheet does not include plasma pressure contribution, this study will substitute the equation of state with an explicit form of the density profile.

In this model, we assume that the asymptotic boundary conditions are known (e.g., determined from spacecraft measurements far away from the discontinuity), including the normal component of the magnetic field (B_z), the magnitude of the magnetic field (B), and the asymptotic properties of the incident fluid streams. It should be noted that while the velocity space boundary between different ion populations may be clearly distinguishable in the uniform field region outside the current sheet[46], this boundary becomes more subtle, diffuse, and less tractable within the current sheet. For instance, an individual ion may transition from one population to another, and some ions may even become trapped within the current sheet (see the discussion in Refs. 50 and 51). These complexities, particularly ion behavior within the sheet, are beyond the scope of this paper and will not be addressed in the current analysis.

III. PLASMA-FIELD EQUATIONS FOR FORCE-FREE CURRENT SHEET

The governing equations for the multifluid collisionless plasma model can be expressed in conservation law form

as follows[52]:

$$\left(\frac{\partial}{\partial t}+\mathbf{u}_\alpha\cdot\nabla\right)n_\alpha=-n_\alpha\nabla\cdot\mathbf{u}_\alpha$$

$$m_\alpha n_\alpha\left(\frac{\partial}{\partial t}+\mathbf{u}_\alpha\cdot\nabla\right)\mathbf{u}_\alpha=-\nabla\cdot\mathbf{P}_\alpha+q_\alpha n_\alpha\left(\mathbf{E}+\mathbf{u}_\alpha\times\mathbf{B}\right)$$

$$\nabla\times\mathbf{B}=\mu_0\mathbf{J} \tag{1}$$

$$\nabla\cdot\mathbf{B}=0$$

where α indicates the particle species (electron and different ion populations), n_α the number density, m_α the mass, q_α the charge, $\mathbf{u}_\alpha$ the bulk velocity, $\mathbf{P}_\alpha$ the pressure tensor, $\mathbf{E}$ the electric field a $\mathbf{B}$ the magnetic induction (magnetic field).

This work focuses on steady-state solutions in the deHoffman-Teller frame, where all partial derivatives with respect to time vanish, i.e., $\frac{\partial}{\partial t}=0$. We further assume that the magnetic field varies only along a single Cartesian coordinate, z. Under these assumptions, the force-free condition simplifies to $B_x^2+B_y^2=B_0^2=\text{const}$, even in the presence of a nonzero B_z, which must also be constant based on Gauss's law. Additionally, electrons can be approximated as a massless charge-neutralizing background, which means that the electrons follow the magnetic field lines $\mathbf{u}_e\times\mathbf{B}=0$. For further simplification, we also assume that the ion populations are gyrotropic, eliminating any non-diagonal terms in the pressure tensor. Furthermore, we consider the ions to be single-charged, meaning that $q_\alpha=e$ for all species.

Under all these assumptions, the conservation of fluid mass, expressed as $d(n_\alpha u_{\alpha z})/dz=0$, integrates to a constant parameter, $\Gamma_\alpha=n_\alpha u_{\alpha z}$. The electron motion is aligned with the magnetic field lines, resulting in $\mathbf{u_e}=\Gamma_e\mathbf{B}/(n_e B_z)$. The momentum equations for each ion species are then given by:

$$\begin{aligned}
m_\alpha\Gamma_\alpha\frac{du_{\alpha x}}{dz}&=e(n_\alpha u_{\alpha y}B_z-\Gamma_\alpha B_y)\\
m_\alpha\Gamma_\alpha\frac{du_{\alpha y}}{dz}&=e(\Gamma_\alpha B_x-n_\alpha u_{\alpha x}B_z)\\
m_\alpha\Gamma_\alpha\frac{du_{\alpha z}}{dz}&=-\frac{dp_\alpha}{dz}+n_\alpha e(-\frac{d\phi}{dz}+u_{\alpha x}B_y-n_\alpha u_{\alpha y}B_x)
\end{aligned} \tag{2}$$

Ampere's law connects the fields and the flow components:

$$\frac{1}{\mu_0}\frac{dB_y}{dz}=-J_x=-\sum_\alpha q_\alpha n_\alpha u_{\alpha x}+en_e u_{ex}=-e\left(nU_x-\Gamma_e\frac{B_x}{B_z}\right) \tag{3}$$

$$\frac{1}{\mu_0}\frac{dB_x}{dz}=J_y=\sum_\alpha q_\alpha n_\alpha u_{\alpha y}-en_e u_{ey}=e\left(nU_y-\Gamma_e\frac{B_y}{B_z}\right) \tag{4}$$

$$0=J_z=\sum_\alpha q_\alpha n_\alpha u_{\alpha z}-en_e u_{ez}=e\left(nU_z-\Gamma_e\right) \tag{5}$$

where $n\equiv\sum_\alpha n_\alpha$ is the total ion density, and $U\equiv\sum_\alpha n_\alpha u_\alpha/n$ is the plasma bulk velocity. Equation (5) allows for the elimination of electron variables $\Gamma_e=\sum_\alpha\Gamma_\alpha$.

This is a system of $3N+2$ equations for $4N+2$ unknowns: B_x, B_y, and N each of n, p, u_x, and u_y. Since we are interested in force-free solutions with $B_x^2+B_y^2=B_0^2=\text{const}$, this condition provides one additional equation for the system. For a system with two ion species, this results in 9 equations for 10 unknowns.

Note that if we assume an adiabatic pressure model, which provides N additional equations connecting $\mathbf{P}_\alpha$ and n_α, this system no longer admits a solution for the force-free current sheet. Therefore, instead of the equation of state, we designate one system parameter as a free parameter. By specifying a particular profile for this free parameter, the remaining equations become solvable.

Under the force-free condition, the magnetic field can be expressed in terms of the rotation angle θ, with $B_x=B_0\cos\theta$ and $B_y=B_0\sin\theta$. From Ampere's law (3) and (4), we have:

$$n(U_xB_y-U_yB_x)=0.$$

Furthermore, the density and bulk velocity can be expressed for each ion species as: $n_\alpha u_{\alpha x}B_y=n_\alpha u_{\alpha y}B_x+C_\alpha$. Summing over all species, the above equation simplifies to $\sum_\alpha C_\alpha=0$. The simplest case is to set $C_\alpha=0$ for all species, which is the case we consider throughout this study:

$$n_\alpha(u_{\alpha x}B_y-u_{\alpha y}B_x)=0 \tag{6}$$

Combining the above equation with the first two equations in (2), we obtain:

$$u_{\alpha x}^2+u_{\alpha y}^2=const$$

This would allow us to express the bulk velocity in terms of the rotation angle θ_α as $u_{\alpha x}=u_\alpha\cos\theta_\alpha$ and $u_{\alpha y}=u_\alpha\sin\theta_\alpha$. By substituting the above expression into our assumption (6), we have:

$$\tan\theta=\tan\theta_\alpha$$

Here we consider the case where $\theta_\alpha=\theta$ for all species, but the same procedure can be applied to the case where $\theta_\alpha=\theta+\pi$ and would give the same results.

The first momentum equation (2) after substituting the above expression becomes:

$$-u_\alpha \sin\theta\ \theta' = \frac{e}{m_\alpha}(n_\alpha u_\alpha \sin\theta\ B_z/\Gamma_\alpha - B_0 \sin\theta)$$

$$\Rightarrow \theta' = \frac{e}{m_\alpha}\left(\frac{B_0}{u_\alpha} - \frac{n_\alpha B_z}{\Gamma_\alpha}\right) \tag{7}$$

where $' = d/dz$.

Note that θ and n_α are dependent variables and $u_\alpha, B_0, B_z, \Gamma_\alpha$ are constants predetermined by the system. So for a given profile of n_α and the boundary condition, we could solve the above equation to get the profile of θ.

Ampere's law (4) after substitution becomes:

$$-B_0 \sin\theta\ \theta' = \mu_0 e\left(\sum n_\alpha u_\alpha \sin\theta - \Gamma_e \sin\theta \frac{B_0}{B_z}\right)$$

$$\Rightarrow \theta' = \mu_0 e\left(\frac{\Gamma_e}{B_z} - \frac{\sum n_\alpha u_\alpha}{B_0}\right) \tag{8}$$

The above equation connects the rotation angle θ to the plasma bulk velocity. By equating the above two equations of θ', we could get an equation connecting the plasma bulk velocity to one specific species:

$$nU = B_0\left(\frac{\Gamma_e}{B_z} + \frac{1}{\mu_0 m_\alpha}\left(\frac{n_\alpha B_z}{\Gamma_\alpha} - \frac{B_0}{u_\alpha}\right)\right)$$

In the asymptotic region (far from the current sheet), as all variables approach constant values, the derivatives must vanish. For momentum equation (2), this means $\Gamma_\alpha B_x(\infty) - n_\alpha(\infty)u_{\alpha x}(\infty)B_z = 0$. For Equation (7), this means $-\frac{n_\alpha(\infty)B_z}{\Gamma_\alpha} + \frac{B_0}{u_\alpha} = 0$. This relates the velocity of each species to the asymptotic density. Rewriting Equation (7) in terms of asymptotic values, we have:

$$\theta' = \frac{eB_z}{m_\alpha \Gamma_\alpha}\left(n_\alpha(\infty) - n_\alpha\right) \tag{9}$$

Conveniently, the center of the current sheet is chosen as the origin $z = 0$, which corresponds to the lower boundary of Equation (7). As a result, the boundary condition for the rotation angle is given by $\theta_\alpha(0) = \pi/2$. Combining the x-component of the momentum equation (2) for different ion populations and Ampere's law in the y-direction (4), under the condition that the constant of integration vanishes at the center of the current sheet, we obtain:

$$B_x B_z = \mu_0 \sum m_\alpha \Gamma_\alpha u_{\alpha,x} \tag{10}$$

Evaluating the above equation in the asymptotic limit and substituting $u_{\alpha x}(\infty)$, we have

$$B_z^2 = \mu_0 \sum m_\alpha \Gamma_\alpha^2 / n_\alpha(\infty) \tag{11}$$

This imposes a constraint on the constant parameters of the system B_z, Γ_α and $n_\alpha(\infty)$. For instance, once Γ_α and $n_\alpha(\infty)$ are defined from boundary conditions, B_z is also determined.

Using this equation, we may express the jump in velocities across the current sheet as:

$$\Delta U_x = \left(\sum_\alpha m_\alpha n_\alpha(\infty)\right)^{-1} \sum_\alpha m_\alpha n_\alpha(\infty)\Delta u_{\alpha x}$$

$$\Delta v_{A,x} = \frac{\Delta B_x}{\sqrt{\mu_0 \sum_\alpha m_\alpha n_\alpha(\infty)}},$$

where $\Delta u_{\alpha x} = u_{\alpha x}(+\infty) - u_{\alpha x}(-\infty)$ and $\Delta B_x = B_x(+\infty) - B_x(-\infty)$ are evaluated in the $z \to \pm\infty$ limits. By substituting the expressions for $u_{\alpha x}(\infty)$ and B_z (11), we derive a simplified relation that links the jump in Alfvén velocity to the jump in plasma bulk velocity along the x-direction:

$$\left(\sum_\alpha \Gamma_\alpha m_\alpha\right)\Delta v_{A,x} = \sqrt{\sum_\alpha m_\alpha n_\alpha(\infty) \sum_\alpha \frac{m_\alpha \Gamma_\alpha^2}{n_\alpha(\infty)}}\,\Delta U_x \tag{12}$$

In the case of a single-fluid plasma, this expression reduces to the simpler $\Delta v_{A,x} = \Delta U_x$ force balance condition for a rotational discontinuity. In the case of a system consisting of two counter-streaming ion fluids with equal mass and equal but opposite velocities in the z-direction, i.e., $m_1 = m_2, u_{z,1}(\infty) = -u_{z,2}(\infty)$, the above expression can be further simplified to:

$$|n_1(\infty) - n_2(\infty)|\Delta v_{A,x} = (n_1(\infty) + n_2(\infty))\Delta U_x \tag{13}$$

IV. RESULTS

The multifluid model developed above is applied here to study a specific plasma system consisting of multiple proton populations, where the ion mass is $m_\alpha = m_p$ and the charge is $q_\alpha = e$ for each species α. We focus on analyzing the effects of the model parameters on the plasma system. To determine the profiles of the main plasma characteristics and magnetic field components, we define a density profile for one of the ion species. For this purpose, we adopt a Lorentzian function with a background density to describe the first ion population:

$$n_1(z) \to n_1(\infty) + \frac{\kappa\Gamma_1}{V_A}\frac{1}{1 + (z/L)^2}$$

where L is the spatial scale of the current sheet, $\Gamma_\alpha \equiv n_\alpha(\infty)u_{z,\alpha}(\infty)$ is an integration constant, $V_A \equiv B_z/\sqrt{\mu_0 m_p n(\infty)}$ is the Alfvén velocity in the z direction,

and κ is a dimensionless quantity that characterizes the magnitude of density variation.

By solving Equation (9) analytically, we obtain the rotation angle profile as:

$$\theta(z) = \frac{\pi}{2} - \frac{e\kappa L B_z \tan^{-1}(z/L)}{m_p V_A}$$

where $eLB_z/m_pV_A = L/d_i$ and d_i is ion (proton) inertial length.

Using this result, the density profiles for the other ion population and the total ion population can be expressed as:

$$n_\alpha(z) = n_\alpha(\infty) + \frac{\Delta n_\alpha}{1+(z/L)^2}$$
$$n(z) = n(\infty) + \frac{\Delta n}{1+(z/L)^2}$$

where $\Delta n_\alpha \equiv n_\alpha(0) - n_\alpha(\infty) = \kappa\Gamma_\alpha/V_A$ and $\Delta n \equiv n(0) - n(\infty) = \kappa\sum_\alpha \Gamma_\alpha/V_A$.

The corresponding models for the magnetic field, current density, and plasma flows are given by:

$$B_x(z) = B_0\cos(\theta(z))$$
$$B_y(z) = B_0\sin(\theta(z))$$
$$\mathbf{J}(z) = \frac{e\kappa B_z}{\mu_0 m_p V_A}\frac{\mathbf{B}(z)}{1+(z/L)^2}$$
$$\mathbf{J}_e(z) = -e\frac{\mathbf{B}(z)}{B_z}\sum_\alpha \Gamma_\alpha$$
$$\mathbf{J}_i(z) = \mathbf{J}(z) - \mathbf{J}_e(z)$$
$$\mathbf{U}(z) = \frac{\mathbf{J}_i(z)}{en(z)}$$

where i and e denote ion and electron currents, and the vectors $\mathbf{J}$, $\mathbf{B}$, $\mathbf{U}$ have two components, x and y. Using the relation $\Delta n_\alpha/\Delta n = \Gamma_\alpha/\sum_\alpha\Gamma_\alpha$ and (11), κ and $\sum_\alpha\Gamma_\alpha$ can be expressed in a form that involves only densities of ion populations:

$$\kappa = \sqrt{\sum_\alpha \frac{\Delta n_\alpha^2}{n(\infty)n_\alpha(\infty)}}$$
$$\sum_\alpha \Gamma_\alpha = \sqrt{\frac{B_z^2}{\mu_0 m_p}\frac{\Delta n^2}{\sum_\alpha \Delta n_\alpha^2/n_\alpha(\infty)}} = \frac{V_A\Delta n}{\kappa}$$

To facilitate subsequent analysis and visualization, it is useful to adopt a dimensionless system by normalizing the variables with their characteristic values: in this study, the magnetic field is normalized by $B_{\rm ref} = B_z$, the density by $n_{\rm ref} = n(\infty)$, the length by $L_{\rm ref} = d_i$, and the velocity by $V_{\rm ref} = V_A$. In these normalized units, the relevant variables take the following form:

$$\theta(z) = \frac{\pi}{2} - \frac{\kappa L\tan^{-1}(z/L)}{d_i}$$
$$\frac{\mathbf{J}}{eV_A n(\infty)} = \frac{\mathbf{B}(z)}{B_z}\frac{\kappa}{1+(z/L)^2}$$
$$\frac{\mathbf{J}_e}{eV_A n(\infty)} = -\frac{\mathbf{B}(z)}{B_z}\frac{\Delta n}{\kappa n(\infty)}$$
$$\frac{\mathbf{U}}{V_A} = \frac{\mathbf{B}(z)}{B_z}\frac{n(\infty)}{n(z)} \cdot \left(\frac{\kappa}{1+(z/L)^2} + \frac{\Delta n}{\kappa n(\infty)}\right)$$

The system is fully determined given κ, $\sum_\alpha\Gamma_\alpha$, L, and B_0 (or equivalently, Δn_α, $n_\alpha(\infty)$, L, and B_0). For the simplest situation where we have two populations of ions of the same density but with oppositely directed bulk velocities in the asymptotic limit, i.e. $n_1(\infty) = n_2(\infty), u_{1z}(\infty) = -u_{2z}(\infty)$, the profile of the magnetic field, plasma density, and plasma velocity for one specific case ($L = d_i, \kappa = 1, B_0 = 2B_z$) is plotted in Figure 2. Note that in this symmetric case with $\sum_\alpha\Gamma_\alpha = 0$, $\Delta n = \Delta n_1 + \Delta n_2 = 0$ we have

$$\mathbf{J} = \frac{\mathbf{B}(z)}{B_z}\frac{eV_A n(\infty)}{1+(z/L)^2}, \quad \mathbf{J}_e = 0, \quad \mathbf{U} = \frac{\mathbf{J}}{en(\infty)}$$

and

$$\theta = \frac{\pi}{2} - \tan^{-1}(z/L)$$

Therefore, we have zero electron current across the current sheet and zero B_y in the asymptotic limit, corresponding to a 180° rotation of the magnetic field across the current sheet. However, in general cases with $\Delta n \neq 0$, we would expect the electron current to be nonzero.

Figure 2 (left) shows a constant density and zero U_z, because for $u_1 = -u_2$ we have $\sum_\alpha\Gamma_\alpha = 0$, which leads to $n = n(\infty)$, $\Delta n = 0$, and $U_z \equiv \sum_\alpha\Gamma_\alpha/n = 0$. Plasma (ion) bulk flow velocities show profiles with U_y peaked at the current sheet center and U_x reversal across the current sheet center. The velocity magnitude goes to zero far away from the current sheet, and there is no velocity jump across the sheet (i.e., this is a current sheet with zero Alfvénicity). Therefore, this solution represents a limiting case when the force-free current sheet with $B_z \neq 0$ has $\Delta U_x = 0$, but Δv_A is balanced by counter-streaming ion beams with $n_1(\infty) - n_2(\infty) = 0$. Substituting into the right side Eq. (13), one can show that the stress balance is satisfied.

Figure 2 (right) shows that in the absence of electron currents, the current density components have the same symmetry as the ion bulk velocity components: $U_x \sim J_x$ and $U_x \sim J_y$.

The magnitude of the velocity jump across the current sheet, ΔU, is directly related to the system parameters. To demonstrate this, we consider the current sheet with finite $B_y(\infty)$. We set $B_y(\infty) = B_0/2, B_0 = 2B_z$, and

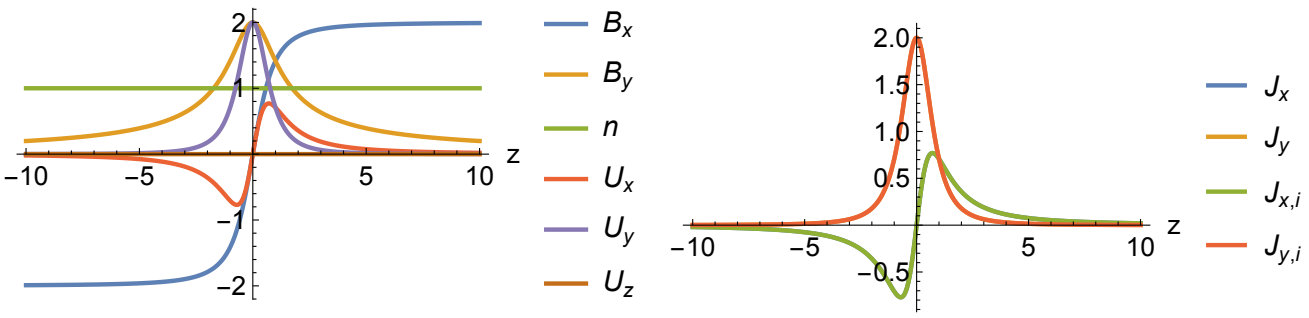

FIG. 2: Left: Magnetic field, ion density, and ion bulk velocity for the case where $n_1 = n_2, u_1 = -u_2$ and $L = d_i, \sum_\alpha \Gamma_\alpha = \Delta n V_A = 1, B_0 = 2B_z$. Right: Current density profiles for the same case. Note that the blue line (J_x) coincides with the green line ($J_{x,i}$), and the yellow line (J_y) coincides with the red line ($J_{y,i}$).

consider two ion populations with opposite bulk velocities but with different densities. By varying $n_1(\infty)$, we find that the magnetic field profiles remain unchanged, while plasma density and velocity profiles exhibit significant variations.

Figure 3 shows the results for $n_1(\infty)/n_2(\infty) = 1.5$. The main (reversal) magnetic field component, B_x, has a profile similar to that of Fig. 2, whereas the peak of B_y is embedded in a constant background. The plasma density and U_z profiles have a small minimum in the current sheet center, and this minimum in density must be compensated by a maximum in ion temperature to maintain constant plasma pressure. Compared with Fig. 2, the ion velocity components do not go to zero at the current sheet boundaries, and we have a finite Alfvénicity with $\Delta U_x = \left|\frac{n_1(\infty)-n_2(\infty)}{n_1(\infty)+n_2(\infty)}\right| \Delta v_{A,x}$.

A finite Δn results in nonzero electron currents. Therefore, the ion current density and the total current density profiles are not identical. There are finite ion and electron currents at the current sheet boundaries, but these currents compensate each other outside the current sheet and leave a nonzero total current only inside the current sheet.

To show how Alfvénicity depends on the current sheet parameters, we show in Fig. 4 (left) profiles of normalized U_x/v_A for different density values, $n_1(\infty)$ of the first ion population (note that $n_1(\infty) = 0.5$ is the symmetric case with $n_1(\infty) = n_2(\infty)$ and $\Delta n = 0$). For $n_1(\infty) = 0.5$, we have zero bulk velocity change across the current sheet and the change increases as $n_1(\infty)$ decreases to zero. Therefore, the model allows regulation of ΔU_x by the density of the ion beam. Figure 4 (right) shows the normalized plasma velocity U_y for different $n_1(\infty)$: There is no jump of U_y across the sheet, but the asymptotic $U_y(\infty)$ depends on n_1 and decreases to zero when $n_1(\infty) = n_2(\infty)$.

The spatial profiles of U_x and U_y follow the profiles of B_x and B_y. Consequently, the ratios $U_x/v_{A,x}$ and $U_y/v_{A,y}$ provide insight into the extent to which variations in the Alfvén velocity can be explained by variations in plasma flow. These ratios are plotted in Figure 5. The normalized plasma velocity profiles are exactly the same for $U_x/v_{A,x}$ and $U_y/v_{A,y}$ and depend only on $n_1(\infty)$. As $n_1(\infty)$ approaches zero, the normalized plasma velocity at the current sheet boundaries tends to unity $U_x/v_{A,x} \to 1$. This suggests that the stress balance in the current sheet under such conditions is equivalent to that of a single-fluid rotational discontinuity.

V. COMPARISON WITH OBSERVATIONS

To demonstrate the potential of this model, we analyze statistical observations of current sheets (solar wind discontinuities) collected in the near-Earth solar wind by the Wind[29] and ARTEMIS[28] missions, as well as in the near-Sun solar wind by Parker Solar Probe[27]. The criteria of current sheet selection and basic methods for analyzing spacecraft measurements can be found in Refs. 53. Figure 6 presents the probability density functions (PDFs) of the velocity ratio $\Delta U_x/\Delta v_{A,x}$ along the maximum variance direction using the minimum variance analysis technique[54]. These PDFs are derived from measurements collected by the PSP, ARTEMIS, and Wind missions during PSP encounter 7 (from 2021-01-14 to 2021-01-21). Each curve represents the distribution of the velocity ratio for a specific dataset, with PSP capturing current sheets near the Sun, while ARTEMIS and Wind capture measurements at approximately 1 AU.

VI. DISCUSSION

This work presents a multifluid model of force-free current sheets with an arbitrary level of Alfvénicity. The primary application of this model is to describe current sheets in the solar wind[55] and planetary magnetotails[56].

In the context of our model, these observations shown in Figure 6 reveal distinct solar wind behaviors at different heliocentric distances. Near the Sun, the velocity ratio (Alfvénicity) is significantly higher, indicating that the configuration of current sheets closely resembles that of a single-fluid discontinuity. Within our model

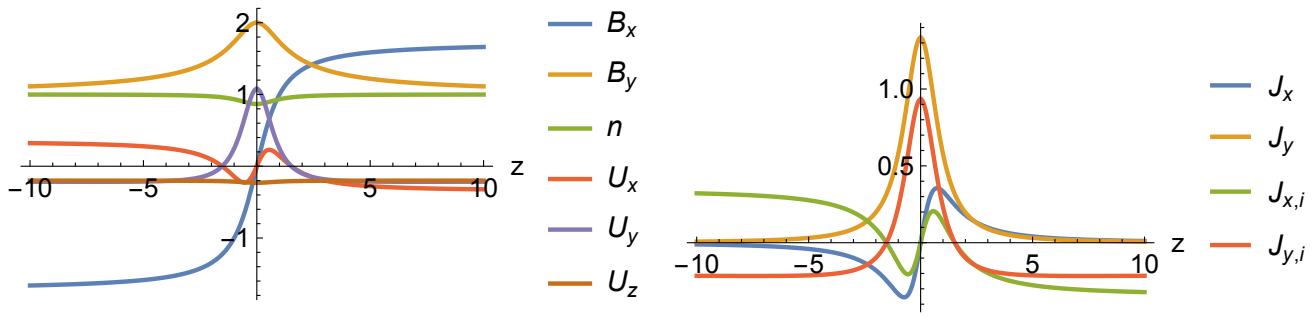

FIG. 3: Same as Figure 2, but for two ion species with same bulk velocity but different densities $n_1(\infty)/n_2(\infty) = 1.5$ and $B_y(\infty) = B_0/2 = B_z$.

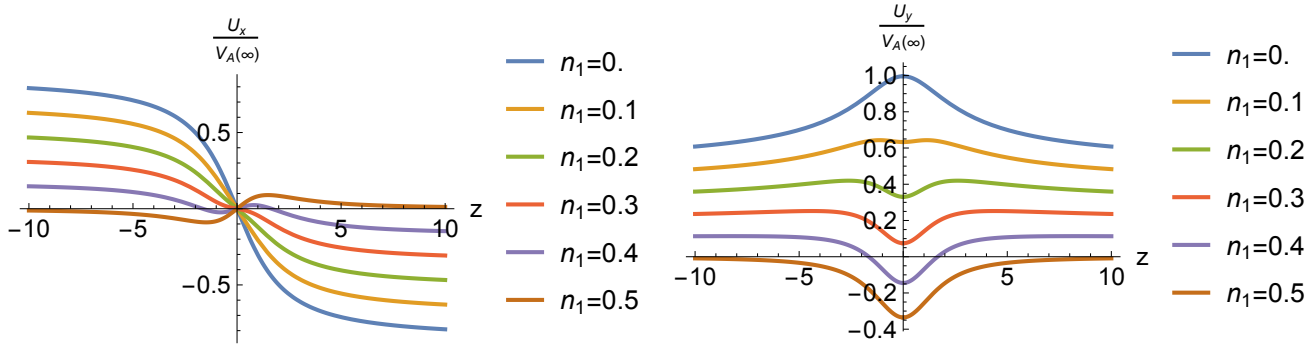

FIG. 4: Plasma velocity U_x (left) and U_y (right) profiles normalized by asymptotic Alfvén velocity $V_A(\infty) = B_0/\sqrt{\mu_0 m_p n(\infty)}$ for different $n_1(\infty)$.

framework, this corresponds to a less balanced state between ion populations, characterized by $n_1 \gg n_2$. In contrast, at 1 AU, as evidenced by the ARTEMIS and Wind datasets, the current sheets exhibit considerably lower Alfvénicity, with $\Delta U_x/\Delta v_{A,x} < 0.5$ (this is a quite typical value for 1 AU; see Refs. 7 and 57). Within our model, such low Alfvénicity suggests more balanced densities of two ion populations, with $n_1 \approx n_2$. Therefore, interpreting the observational dataset within the framework of our model, we propose that as the solar wind propagates outward and transports current sheets, the balance between the densities of ion populations (n_1 and n_2) evolves. This transition occurs from a single-fluid-dominated regime near the Sun to a more balanced multifluid regime at greater distances. This conclusion, of course, is based on a simplified treatment of the model equations. However, in contrast to single-fluid models (with and without anisotropy), our multifluid approach offers a potential explanation for the observed low Alfvénicity in the distant solar wind.

DATA AVAILABILITY

The codes and data that support the findings of this study are available in the GitHub repository `https://github.com/Beforerr/cs_theory`.

[1] B. J. Vasquez, V. I. Abramenko, D. K. Haggerty, and C. W. Smith, "Numerous small magnetic field discontinuities of Bartels rotation 2286 and the potential role of Alfvénic turbulence," Journal of Geophysical Research (Space Physics) **112**, A11102 (2007).

[2] A. Greco, S. Perri, S. Servidio, E. Yordanova, and P. Veltri, "The Complex Structure of Magnetic Field Discontinuities in the Turbulent Solar Wind," Astrophys. J. Lett. **823**, L39 (2016), arXiv:1511.03084 [astro-ph.SR].

[3] J. J. Podesta, "The most intense current sheets in the high-speed solar wind near 1 AU," J. Geophys. Res. **122**, 2795–2823 (2017).

[4] I. Y. Vasko, K. Alimov, T. Phan, S. D. Bale, F. S. Mozer, and A. V. Artemyev, "Kinetic-scale Current Sheets in the Solar Wind at 1 au: Scale-dependent Properties and Critical Current Density," Astrophys. J. Lett. **926**, L19 (2022), arXiv:2112.15256 [physics.space-ph].

[5] J. De Keyser, M. Roth, and A. Söding, "Flow shear across solar wind discontinuities: WIND observations," Geophys. Res. Lett. **25**, 2649–2652 (1998).

[6] G. Paschmann, S. Haaland, B. Sonnerup, and T. Knetter, "Discontinuities and Alfvenic fluctuations in the solar wind," Annales Geophysicae **31**, 871–887 (2013).

[7] A. V. Artemyev, V. Angelopoulos, and I. Y. Vasko, "Kinetic properties of solar wind discontinuities at 1 AU observed by ARTEMIS," Journal of Geophysical Research: Space Physics **124**, 3858–3870 (2019).

[8] R. D'Amicis, D. Perrone, R. Bruno, and M. Velli, "On Alfvénic Slow Wind: A Journey From the Earth Back to the Sun," Journal of Geophysical Research: Space Physics **126**, e2020JA028996 (2021).

[9] M. V. Medvedev, P. H. Diamond, V. I. Shevchenko, and V. L. Galinsky, "Dissipative Dynamics of Collisionless Nonlin-

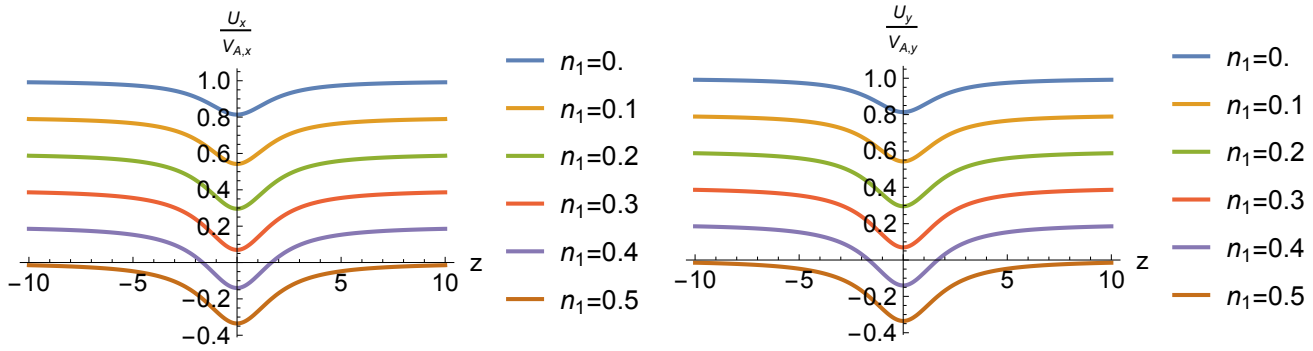

FIG. 5: Plasma velocity U_x (left) and U_y (right) profiles normalized by local Alfvén velocity $v_{A,x}(z) = B_x(z)/\sqrt{\mu_0 m_p n(z)}$ and $v_{A,y}(z) = B_y(z)/\sqrt{\mu_0 m_p n(z)}$ for different $n_1(\infty)$.

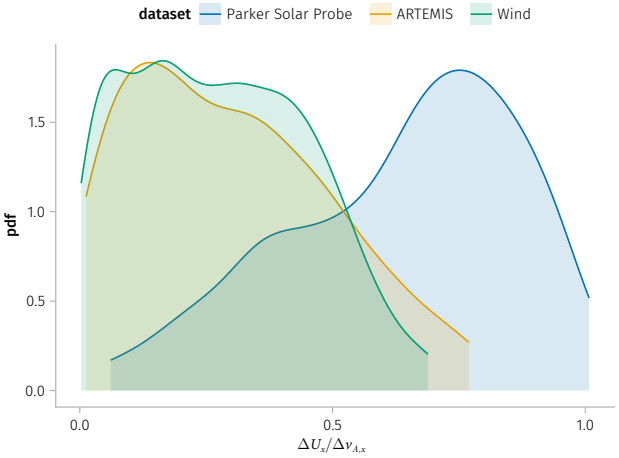

FIG. 6: Statistics of the asymptotic velocity ratio from PSP, Wind, and ARTEMIS spacecraft observations during PSP encounter 7 period from 2021-01-14 to 2021-01-21.

ear Alfvén Wave Trains," Physical Review Letters **78**, 4934–4937 (1997), physics/9707021.

[10] M. V. Medvedev and P. H. Diamond, "Fluid models for kinetic effects on coherent nonlinear Alfvén waves. I. Fundamental theory," Physics of Plasmas **3**, 863–873 (1996), physics/9612017.

[11] S. Servidio, A. Greco, W. H. Matthaeus, K. T. Osman, and P. Dmitruk, "Statistical association of discontinuities and reconnection in magnetohydrodynamic turbulence," J. Geophys. Res. **116**, A09102 (2011).

[12] T. Neukirch, F. Wilson, and O. Allanson, "A family of Vlasov Maxwell equilibrium distribution functions describing a transition from the Harris sheet to the force-free Harris sheet," Journal of Plasma Physics **86**, 825860302 (2020), arXiv:2005.10238 [physics.plasm-ph].

[13] R. Nakamura, W. Baumjohann, M. Fujimoto, Y. Asano, A. Runov, C. J. Owen, A. N. Fazakerley, B. Klecker, H. Rème, E. A. Lucek, M. Andre, and Y. Khotyaintsev, "Cluster observations of an ion-scale current sheet in the magnetotail under the presence of a guide field," J. Geophys. Res. **113**, A07S16 (2008).

[14] S. R. Kamaletdinov, A. V. Artemyev, A. Runov, and V. Angelopoulos, "Thin Current Sheets in the Magnetotail at Lunar Distances: Statistics of ARTEMIS Observations," Journal of Geophysical Research (Space Physics) **129**, e2023JA032130 (2024).

[15] G. A. DiBraccio, J. R. Espley, J. R. Gruesbeck, J. E. P. Connerney, D. A. Brain, J. S. Halekas, D. L. Mitchell, J. P. McFadden, Y. Harada, R. Livi, G. Collinson, T. Hara, C. Mazelle, and B. M. Jakosky, "Magnetotail dynamics at Mars: Initial MAVEN observations," Geophys. Res. Lett. **42**, 8828–8837 (2015).

[16] A. V. Artemyev, V. Angelopoulos, J. S. Halekas, A. Runov, L. M. Zelenyi, and J. P. McFadden, "Mars's magnetotail: Nature's current sheet laboratory," J. Geophys. Res. **122**, 5404–5417 (2017).

[17] Z. J. Rong, S. Barabash, G. Stenberg, Y. Futaana, T. L. Zhang, W. X. Wan, Y. Wei, X. D. Wang, L. H. Chai, and J. Zhong, "The flapping motion of the Venusian magnetotail: Venus Express observations," J. Geophys. Res. **120**, 5593–5602 (2015).

[18] Z. J. Rong, Y. Ding, J. A. Slavin, J. Zhong, G. Poh, W. J. Sun, Y. Wei, L. H. Chai, W. X. Wan, and C. Shen, "The Magnetic Field Structure of Mercury's Magnetotail," Journal of Geophysical Research (Space Physics) **123**, 548–566 (2018).

[19] A. V. Artemyev, I. Y. Vasko, and S. Kasahara, "Thin current sheets in the Jovian magnetotail." Plan. Sp. Sci. **96**, 133–145 (2014).

[20] E. V. Panov, A. V. Artemyev, R. Nakamura, and W. Baumjohann, "Two Types of Tangential Magnetopause Current Sheets: Cluster Observations and Theory," J. Geophys. Res. **116**, A12204 (2011).

[21] A. S. Lukin, E. V. Panov, A. V. Artemyev, A. A. Petrukovich, S. Haaland, R. Nakamura, V. Angelopoulos, A. Runov, E. V. Yushkov, L. A. Avanov, B. L. Giles, C. T. Russell, and R. J. Strangeway, "Comparison of the Flank Magnetopause at Near-Earth and Lunar Distances: MMS and ARTEMIS Observations," Journal of Geophysical Research (Space Physics) **125**, e28406 (2020).

[22] F. Wilson, T. Neukirch, M. Hesse, M. G. Harrison, and C. R. Stark, "Particle-in-cell simulations of collisionless magnetic reconnection with a non-uniform guide field," Physics of Plasmas **23**, 032302 (2016), arXiv:1512.07844 [astro-ph.SR].

[23] C. Shi, A. Artemyev, M. Velli, and A. Tenerani, "Stability of the Magnetotail Current Sheet With Normal Magnetic Field and Field-Aligned Plasma Flows," Journal of Geophysical Research (Space Physics) **126**, e29711 (2021).

[24] A. V. Artemyev, A. I. Neishtadt, A. A. Vasiliev, V. Angelopoulos, A. A. Vinogradov, and L. M. Zelenyi, "Superfast ion scattering by solar wind discontinuities," Phys. Rev. E **102**, 033201 (2020).

[25] F. Malara, S. Perri, and G. Zimbardo, "Charged-particle chaotic dynamics in rotational discontinuities," Physical Review E **104**, 025208 (2021).

[26] F. Malara, S. Perri, J. Giacalone, and G. Zimbardo, "Energetic particle dynamics in a simplified model of a solar wind magnetic switchback," Astronomy & Astrophysics **677**, A69 (2023).

[27] N. J. Fox, M. C. Velli, S. D. Bale, R. Decker, A. Driesman, R. A. Howard, J. C. Kasper, J. Kinnison, M. Kusterer, D. Lario,

M. K. Lockwood, D. J. McComas, N. E. Raouafi, and A. Szabo, "The solar probe plus mission: Humanity's first visit to our star," Space Science Reviews **204**, 7–48 (2016).
[28]V. Angelopoulos, "The ARTEMIS Mission," Space Science Reviews **165**, 3–25 (2011).
[29]M. H. Acuña, K. W. Ogilvie, D. N. Baker, S. A. Curtis, D. H. Fairfield, and W. H. Mish, "The Global Geospace Science Program and Its Investigations," Space Science Reviews **71**, 5–21 (1995).
[30]S. D. Bale, K. Goetz, P. R. Harvey, P. Turin, J. W. Bonnell, T. Dudok de Wit, R. E. Ergun, R. J. MacDowall, M. Pulupa, M. Andre, M. Bolton, J.-L. Bougeret, T. A. Bowen, D. Burgess, C. A. Cattell, B. D. G. Chandran, C. C. Chaston, C. H. K. Chen, M. K. Choi, J. E. Connerney, S. Cranmer, M. Diaz-Aguado, W. Donakowski, J. F. Drake, W. M. Farrell, P. Fergeau, J. Fermin, J. Fischer, N. Fox, D. Glaser, M. Goldstein, D. Gordon, E. Hanson, S. E. Harris, L. M. Hayes, J. J. Hinze, J. V. Hollweg, T. S. Horbury, R. A. Howard, V. Hoxie, G. Jannet, M. Karlsson, J. C. Kasper, P. J. Kellogg, M. Kien, J. A. Klimchuk, V. V. Krasnoselskikh, S. Krucker, J. J. Lynch, M. Maksimovic, D. M. Malaspina, S. Marker, P. Martin, J. Martinez-Oliveros, J. McCauley, D. J. McComas, T. McDonald, N. Meyer-Vernet, M. Moncuquet, S. J. Monson, F. S. Mozer, S. D. Murphy, J. Odom, R. Oliverson, J. Olson, E. N. Parker, D. Pankow, T. Phan, E. Quataert, T. Quinn, S. W. Ruplin, C. Salem, D. Seitz, D. A. Sheppard, A. Siy, K. Stevens, D. Summers, A. Szabo, M. Timofeeva, A. Vaivads, M. Velli, A. Yehle, D. Werthimer, and J. R. Wygant, "The FIELDS Instrument Suite for Solar Probe Plus," Space Science Reviews **204**, 49–82 (2016).
[31]J. C. Kasper, R. Abiad, G. Austin, M. Balat-Pichelin, S. D. Bale, J. W. Belcher, P. Berg, H. Bergner, M. Berthomier, J. Bookbinder, E. Brodu, D. Caldwell, A. W. Case, B. D. G. Chandran, P. Cheimets, J. W. Cirtain, S. R. Cranmer, D. W. Curtis, P. Daigneau, G. Dalton, B. Dasgupta, D. DeTomaso, M. Diaz-Aguado, B. Djordjevic, B. Donaskowski, M. Effinger, V. Florinski, N. Fox, M. Freeman, D. Gallagher, S. P. Gary, T. Gauron, R. Gates, M. Goldstein, L. Golub, D. A. Gordon, R. Gurnee, G. Guth, J. Halekas, K. Hatch, J. Heerikuisen, G. Ho, Q. Hu, G. Johnson, S. P. Jordan, K. E. Korreck, D. Larson, A. J. Lazarus, G. Li, R. Livi, M. Ludlam, M. Maksimovic, J. P. McFadden, W. Marchant, B. A. Maruca, D. J. McComas, L. Messina, T. Mercer, S. Park, A. M. Peddie, N. Pogorelov, M. J. Reinhart, J. D. Richardson, M. Robinson, I. Rosen, R. M. Skoug, A. Slagle, J. T. Steinberg, M. L. Stevens, A. Szabo, E. R. Taylor, C. Tiu, P. Turin, M. Velli, G. Webb, P. Whittlesey, K. Wright, S. T. Wu, and G. Zank, "Solar Wind Electrons Alphas and Protons (SWEAP) Investigation: Design of the Solar Wind and Coronal Plasma Instrument Suite for Solar Probe Plus," Space Science Reviews **204**, 131–186 (2016).
[32]H. U. Auster, K. H. Glassmeier, W. Magnes, O. Aydogar, W. Baumjohann, D. Constantinescu, D. Fischer, K. H. Fornacon, E. Georgescu, P. Harvey, O. Hillenmaier, R. Kroth, M. Ludlam, Y. Narita, R. Nakamura, K. Okrafka, F. Plaschke, I. Richter, H. Schwarzl, B. Stoll, A. Valavanoglou, and M. Wiedemann, "The THEMIS fluxgate magnetometer," Space Science Reviews **141**, 235–264 (2008).
[33]J. P. McFadden, C. W. Carlson, D. Larson, M. Ludlam, R. Abiad, B. Elliott, P. Turin, M. Marckwordt, and V. Angelopoulos, "The THEMIS ESA plasma instrument and In-flight calibration," in *The THEMIS Mission*, edited by J. L. Burch and V. Angelopoulos (Springer, New York, NY, 2009) pp. 277–302.
[34]R. P. Lepping, M. H. Acũna, L. F. Burlaga, W. M. Farrell, J. A. Slavin, K. H. Schatten, F. Mariani, N. F. Ness, F. M. Neubauer, Y. C. Whang, J. B. Byrnes, R. S. Kennon, P. V. Panetta, J. Scheifele, and E. M. Worley, "The WIND magnetic field investigation," Space Science Reviews **71**, 207–229 (1995).
[35]K. W. Ogilvie, D. J. Chornay, R. J. Fritzenreiter, F. Hunsaker, J. Keller, J. Lobell, G. Miller, J. D. Scudder, E. C. Sittler, R. B. Torbert, D. Bodet, G. Needell, A. J. Lazarus, J. T. Steinberg, J. H. Tappan, A. Mavretic, and E. Gergin, "SWE, a comprehensive plasma instrument for the WIND spacecraft," Space Science Reviews **71**, 55–77 (1995).
[36]M. G. Harrison and T. Neukirch, "One-Dimensional Vlasov-Maxwell Equilibrium for the Force-Free Harris Sheet," Physical Review Letters **102**, 135003 (2009), arXiv:0812.1240 [physics.plasm-ph].
[37]O. Allanson, T. Neukirch, F. Wilson, and S. Troscheit, "An exact collisionless equilibrium for the Force-Free Harris Sheet with low plasma beta," Physics of Plasmas **22**, 102116 (2015), arXiv:1510.07667 [physics.plasm-ph].
[38]O. Allanson, T. Neukirch, S. Troscheit, and F. Wilson, "From one-dimensional fields to Vlasov equilibria: theory and application of Hermite polynomials," Journal of Plasma Physics **82**, 905820306 (2016), arXiv:1606.01661 [physics.plasm-ph].
[39]T. Neukirch, I. Y. Vasko, A. V. Artemyev, and O. Allanson, "Kinetic Models of Tangential Discontinuities in the Solar Wind," Astrophys. J. **891**, 86 (2020), arXiv:2001.11380 [physics.space-ph].
[40]P. D. Hudson, "Discontinuities in an anisotropic plasma and their identification in the solar wind," Plan. Sp. Sci. **18**, 1611–1622 (1970).
[41]A. Tenerani, M. Velli, and P. Hellinger, "The Parametric Instability of Alfvén Waves: Effects of Temperature Anisotropy," Astrophys. J. **851**, 99 (2017), arXiv:1711.06371 [physics.space-ph].
[42]A. Tenerani and M. Velli, "Nonlinear Firehose Relaxation and Constant-B Field Fluctuations," Astrophys. J. Lett. **867**, L26 (2018), arXiv:1808.04453 [physics.plasm-ph].
[43]B. Abraham-Shrauner, "Propagation of hydromagnetic waves through an anisotropic plasma," Journal of Plasma Physics **1**, 361–378 (1967).
[44]E. N. Parker, "Dynamical Instability in an Anisotropic Ionized Gas of Low Density," Physical Review **109**, 1874–1876 (1958).
[45]R. Z. Sagdeev and V. D. Shafranov, "On the Instability of a Plasma with an Anisotropic Distribution of Velocities in a Magnetic Field," Soviet Phys. JETP **12**, 130–132 (1961).
[46]A. V. Artemyev, V. Angelopoulos, I. Y. Vasko, and L. M. Zelenyi, "Ion Nongyrotropy in Solar Wind Discontinuities," Astrophys. J. Lett. **889**, L23 (2020).
[47]Y. Shen, A. Artemyev, V. Angelopoulos, T. Z. Liu, and I. Vasko, "Comparing Plasma Anisotropy Associated with Solar Wind Discontinuities and Alfvénic Fluctuations," Astrophys. J. **961**, 41 (2024).
[48]I. Y. Vasko, A. V. Artemyev, A. A. Petrukovich, and H. V. Malova, "Thin current sheets with strong bell-shape guide field: Cluster observations and models with beams," Annales Geophysicae **32**, 1349–1360 (2014).
[49]L. C. Steinhauer, M. P. McCarthy, and E. C. Whipple, "Multifluid model of a one-dimensional steady state magnetotail current sheet," Journal of Geophysical Research: Space Physics **113** (2008), 10.1029/2007JA012578.
[50]A. V. Artemyev, "A model of one-dimensional current sheet with parallel currents and normal component of magnetic field," Physics of Plasmas **18**, 022104 (2011).
[51]O. V. Mingalev, I. V. Mingalev, M. N. Mel'nik, A. V. Artemyev, H. V. Malova, V. Y. Popov, S. Chao, and L. M. Zelenyi, "Kinetic models of current sheets with a sheared magnetic field," Plasma Physics Reports **38**, 300–314 (2012).
[52]I. P. Shkarofsky, T. W. Johnston, and M. P. Bachnynski, *The particle kinetic of plasmas* (Addison-wesley Piblishing company, 1966).
[53]Z. Zhang, A. V. Artemyev, V. Angelopoulos, and I. Vasko, "Solar wind discontinuities in the outer heliosphere: Spatial distribution between 1 and 5 AU," (2025).
[54]B. U. Ö. Sonnerup and M. Scheible, *Cluster-II Workshop Multiscale / Multipoint Plasma Measurements*, edited by G.Paschmann and Patrick W. D. , ESA Special Publication, Vol. 449 (2000).
[55]A. V. Artemyev, V. Angelopoulos, I.-Y. Vasko, A. Runov, L. A. Avanov, B. L. Giles, C. T. Russell, and R. J. Strangeway, "On

the kinetic nature of solar wind discontinuiti," Geophys. Res. Lett. **46**, 1185–1194 (2019).
[56]S. R. Kamaletdinov, A. V. Artemyev, A. Runov, and V. Angelopoulos, "Characteristics of Thin Magnetotail Current Sheet Plasmas at Lunar Distances," Journal of Geophysical Research (Space Physics) **129**, e2024JA032755 (2024).
[57]J. De Keyser and M. Roth, "Equilibrium conditions and magnetic field rotation at the tangential discontinuity magnetopause," J. Geophys. Res. **103**, 6653–6662 (1998).